Assessment of Crack Tip Plastic Zone Size and Shape and its Influence on Crack Tip Shielding

J M Vasco-Olmo[1], M N James[2, 3], C J Christopher[2], E A Patterson[4] and F A Díaz[1]

[1]Departamento de Ingeniería Mecánica y Minera, University of Jaén, Jaén, Spain.

[2]School of Marine Science & Engineering, University of Plymouth, Plymouth, England.

[3]Department of Mechanical Engineering, Nelson Mandela Metropolitan University, Port Elizabeth, South Africa.

[4]School of Engineering, University of Liverpool, Liverpool, England.

Abstract

This paper presents a novel methodology for the experimental quantification of the crack tip plastic zone during fatigue crack growth. It is based on the application of yielding criteria to estimate the area and shape of the crack tip plastic zone using both the von Mises and Tresca yield criteria. The technique employs strain maps calculated from displacements fields obtained by digital image correlation (DIC). Stress maps were subsequently found by applying these yield criteria. Fatigue cracks were grown in compact tension (CT) specimens made from commercially pure titanium at *R*-ratios of 0.1 and 0.6 and the ability was explored of three different analytical elastic crack tip displacement models (Westergaard, Williams and CJP[1]), to predict shape and size of the crack tip plastic zone. This analysis indicated that the CJP model provided the most accurate prediction of the experimentally obtained plastic zone size and shape.

Keywords: crack tip plastic zone, fatigue, crack tip stress field, crack shielding, stress intensity factor.

Nomenclature:

A, B, C, F, H:	coefficients on the CJP model for describing crack tip displacement fields
a:	crack length
G:	shear modulus
i:	square root of -1
K_F:	opening mode stress intensity factor in the CJP model
K_I:	mode I stress intensity factor
K_R:	retardation stress intensity factor
K_S:	shear stress intensity factor
R:	ratio between the minimum and the maximum applied load
r, θ:	polar coordinates of the collected data points
T_x, T_y:	components of the T-stress in x and y-directions, respectively
u, v:	components of the displacement vector
E:	Young's modulus
z:	complex coordinate of the collected points around the crack tip
ε_{xx}, ε_{yy}, ε_{xy}:	strain fields
κ:	function of Poisson's ratio
ν:	Poisson's ratio
σ_x, σ_y, τ_{xy}:	crack tip stress fields
σ_{0x}:	T-stress

1. Introduction

It has long been recognised in the fracture mechanics community that identifying plastic zone shape and size, and any influences of the plastic zone on a growing fatigue crack is relatively complex whether attempted by simulation or experiment. In simulation work, predictions are usually based on a purely elastic theoretical modelling of crack tip stress fields. Experimentally, determination of the plastically deformed region surrounding a growing fatigue crack has been pursued using a variety of techniques to identify the dimensions of crack tip plastic zones. Uğuz and Martin [2] provide a useful review of the early experimental work on characterising the crack tip plastic zone; this includes techniques based on microhardness measurements, etching, optical interference, micro-strain gauge and electron microscopy. Modern numerical modelling techniques and advanced experimental techniques, including synchrotron diffraction and tomography [3], digital image correlation (DIC) [4], thermography [5] and electron backscatter diffraction (EBSD) [6] have started to unlock the potential of full-field measurements in determining crack tip stress intensity factors, residual stresses, strains and hence plastic zone dimensions.

However, most reported work has used existing models of crack tip stress fields and plastic deformation, e.g. strip yield models of crack closure [4] or elastic models based on the Williams' solution for crack tip stresses [7]. There is clearly scope for combining full field measurement techniques with an improved model of the crack tip stress field that attempts to better incorporate the influence on the elastic stress field driving growth, of any stresses induced by the plastically deformed region that surrounds a growing fatigue crack.

Some of the present authors have previously proposed such a model [1] based on a modified version of the Williams' crack tip stress field. The premise underlying the modified model is that the elastic stress field that drives crack growth is controlled by the applied loading and also influenced by the boundary stresses imposed at its interface with the plastic zone. These induced boundary stresses represent both the effect of contact in the crack wake and the effect of compatibility-induced shear stresses that arise at the interface of the elastic field with the plastic enclave that surrounds a growing fatigue crack. The model was initially based on full-field stress measurements made using photoelasticity in polycarbonate compact tension specimens but has been subsequently extended to cover biaxial displacement measurements on metallic specimens using DIC [8].

The objective of the current work is the experimental determination of the plastic zone size and shape via DIC in titanium compact tension specimens, and then to evaluate the capability of three crack tip field models to characterise stress or displacement and hence to predict plastic zone size and shape. The three models considered in this work are the Westergaard crack tip

stress equations, Williams' expansion series for crack tip stresses and the recently developed CJP model [1] for crack tip displacement.

Westergaard equations

In the Westergaard equations, the stress field around the crack tip [9] is described using the stress intensity factors (SIFs), K_I and K_{II}, the T-stress (σ_{0x}) and a polar coordinate system with its origin at the crack tip. Crack tip stress fields are then defined as:

$$\begin{Bmatrix}\sigma_x\\ \sigma_y\\ \tau_{xy}\end{Bmatrix}=\frac{K_I}{\sqrt{2\pi r}}\cos\frac{\theta}{2}\begin{Bmatrix}1-\sin\frac{\theta}{2}\sin\frac{3\theta}{2}\\ 1+\sin\frac{\theta}{2}\sin\frac{3\theta}{2}\\ \sin\frac{\theta}{2}\cos\frac{3\theta}{2}\end{Bmatrix}+\frac{K_{II}}{\sqrt{2\pi r}}\begin{Bmatrix}-\sin\frac{\theta}{2}\left(2+\cos\frac{\theta}{2}\cos\frac{3\theta}{2}\right)\\ \sin\frac{\theta}{2}\cos\frac{\theta}{2}\sin\frac{3\theta}{2}\\ \cos\frac{\theta}{2}\left(1-\sin\frac{\theta}{2}\sin\frac{3\theta}{2}\right)\end{Bmatrix}+\begin{Bmatrix}\sigma_{0x}\\ 0\\ 0\end{Bmatrix} \quad (1)$$

In a similar way, crack tip displacement fields [9] are described as:

$$\begin{Bmatrix}u\\ v\end{Bmatrix}=\frac{K_I}{2G}\sqrt{\frac{r}{2\pi}}\begin{Bmatrix}\cos\frac{\theta}{2}\left(\kappa-1+2\sin^2\frac{\theta}{2}\right)\\ \sin\frac{\theta}{2}\left(\kappa+1-2\cos^2\frac{\theta}{2}\right)\end{Bmatrix}+\frac{K_{II}}{2G}\sqrt{\frac{r}{2\pi}}\begin{Bmatrix}\sin\frac{\theta}{2}\left(\kappa+1+2\cos^2\frac{\theta}{2}\right)\\ \cos\frac{\theta}{2}\left(\kappa-1-2\sin^2\frac{\theta}{2}\right)\end{Bmatrix}+\frac{\sigma_{0x}}{8G}r\begin{Bmatrix}(\kappa+1)\cos\theta\\ (\kappa-3)\sin\theta\end{Bmatrix} \quad (2)$$

Where $G=\frac{E}{2(1+\nu)}$ is the shear modulus, E and ν are the Young's modulus and Poisson's ratio of the material respectively, and $\kappa=\frac{3-\nu}{1+\nu}$ for plane stress or $\kappa=3-4\nu$ for plane strain.

Williams' crack tip stress expansion

According to the Williams' series expansion, crack tip stress fields [10] are expressed as a function of a number of terms in the series, the series coefficients and a polar coordinate system with its origin at the crack tip:

$$\begin{Bmatrix}\sigma_x\\ \sigma_y\\ \tau_{xy}\end{Bmatrix}=\sum_{n=1}^{\infty}\frac{n}{2}A_{In}r^{\frac{n-2}{2}}\begin{Bmatrix}\left[2+(-1)^n+\frac{n}{2}\right]\cos\left(\frac{n}{2}-1\right)\theta-\left(\frac{n}{2}-1\right)\cos\left(\frac{n}{2}-3\right)\theta\\ \left[2-(-1)^n-\frac{n}{2}\right]\cos\left(\frac{n}{2}-1\right)\theta+\left(\frac{n}{2}-1\right)\cos\left(\frac{n}{2}-3\right)\theta\\ -\left[(-1)^n+\frac{n}{2}\right]\sin\left(\frac{n}{2}-1\right)\theta+\left(\frac{n}{2}-1\right)\sin\left(\frac{n}{2}-3\right)\theta\end{Bmatrix}$$
$$-\sum_{n=1}^{\infty}\frac{n}{2}A_{IIn}r^{\frac{n-2}{2}}\begin{Bmatrix}\left[2-(-1)^n+\frac{n}{2}\right]\sin\left(\frac{n}{2}-1\right)\theta-\left(\frac{n}{2}-1\right)\sin\left(\frac{n}{2}-3\right)\theta\\ \left[2+(-1)^n-\frac{n}{2}\right]\sin\left(\frac{n}{2}-1\right)\theta+\left(\frac{n}{2}-1\right)\sin\left(\frac{n}{2}-3\right)\theta\\ -\left[(-1)^n-\frac{n}{2}\right]\cos\left(\frac{n}{2}-1\right)\theta-\left(\frac{n}{2}-1\right)\cos\left(\frac{n}{2}-3\right)\theta\end{Bmatrix} \quad (3)$$

Where $A_{I1}=\frac{K_I}{\sqrt{2\pi}}$, $A_{II1}=-\frac{K_{II}}{\sqrt{2\pi}}$ and $A_{I2}=-\frac{\sigma_{0x}}{4}$. Crack tip displacement fields [11] are defined as:

$$\begin{Bmatrix}u\\ v\end{Bmatrix}=\sum_{n=1}^{\infty}\frac{r^{n/2}}{2G}a_n\begin{Bmatrix}\left[\kappa+\frac{n}{2}+(-1)^n\right]\cos\frac{n\theta}{2}-\frac{n}{2}\cos\frac{(n-4)\theta}{2}\\ \left[\kappa-\frac{n}{2}-(-1)^n\right]\sin\frac{n\theta}{2}+\frac{n}{2}\sin\frac{(n-4)\theta}{2}\end{Bmatrix}$$
$$+\sum_{n=1}^{\infty}\frac{r^{n/2}}{2G}b_n\begin{Bmatrix}-\left[\kappa+\frac{n}{2}-(-1)^n\right]\sin\frac{n\theta}{2}-\frac{n}{2}\sin\frac{(n-4)\theta}{2}\\ \left[\kappa-\frac{n}{2}+(-1)^n\right]\cos\frac{n\theta}{2}+\frac{n}{2}\cos\frac{(n-4)\theta}{2}\end{Bmatrix} \quad (4)$$

Where $a_1=\frac{K_I}{\sqrt{2\pi}}$, $b_1=-\frac{K_{II}}{\sqrt{2\pi}}$ and $a_2=\frac{\sigma_{0x}}{4}$.

CJP model

The CJP model is a novel mathematical model developed by Christopher, James and Patterson [1] based on Muskhelishvili complex potentials [12]. The authors postulated that the plastic enclave which exists around the tip of a fatigue crack and along its flanks will shield the crack from the full influence of the applied elastic stress field and that crack tip shielding includes the effect of crack flank contact forces (so-called crack closure) as well as a compatibility-induced interfacial shear stress at the elastic-plastic boundary. Christopher et al. [1] provided a schematic free-body diagram that is repeated here as Figure 1, which illustrates the forces believed to be acting at the interface between the plastic zone and the surrounding elastic material. In the original formulation of this model, crack tip stress fields [1] were characterised as:

$$
\begin{aligned}
\sigma_x &= -\frac{1}{2}(A+4B+8F)r^{-\frac{1}{2}}\cos\frac{\theta}{2} - \frac{1}{2}Br^{-\frac{1}{2}}\cos\frac{5\theta}{2} - C \\
&\quad -\frac{1}{2}Fr^{-\frac{1}{2}}\left[\ln(r)\left(\cos\frac{5\theta}{2}+3\cos\frac{\theta}{2}\right)+\theta\left(\sin\frac{5\theta}{2}+3\sin\frac{\theta}{2}\right)\right]+O\left(r^{\frac{1}{2}}\right) \\
\sigma_y &= \frac{1}{2}(A-4B-8F)r^{-\frac{1}{2}}\cos\frac{\theta}{2} + \frac{1}{2}Br^{-\frac{1}{2}}\cos\frac{5\theta}{2} + H \\
&\quad +\frac{1}{2}Fr^{-\frac{1}{2}}\left[\ln(r)\left(\cos\frac{5\theta}{2}-5\cos\frac{\theta}{2}\right)+\theta\left(\sin\frac{5\theta}{2}-5\sin\frac{\theta}{2}\right)\right]+O\left(r^{\frac{1}{2}}\right) \\
\sigma_{xy} &= -\frac{1}{2}r^{-\frac{1}{2}}\left(A\sin\frac{\theta}{2}+B\sin\frac{5\theta}{2}\right) \\
&\quad -Fr^{-\frac{1}{2}}\sin\theta\left[\ln(r)\cos\frac{3\theta}{2}+\theta\sin\frac{3\theta}{2}\right]+O\left(r^{\frac{1}{2}}\right)
\end{aligned}
\tag{5}
$$

Five coefficients (*A*, *B*, *C*, *F* and *H*) are therefore used to define the stress fields around the crack tip.

This model can be also solved in terms of displacement [1]:

$$
\begin{aligned}
2G(u+iv) &= \kappa\left[-2(B+2F)z^{\frac{1}{2}}+4Fz^{\frac{1}{2}}-2Fz^{\frac{1}{2}}\ln(z)-\frac{C-H}{4}z\right] \\
&\quad -z\left[-(B+2F)\bar{z}^{-\frac{1}{2}}-F\bar{z}^{-\frac{1}{2}}\overline{\ln(z)}-\frac{C-H}{4}\right] \\
&\quad -\left[A\bar{z}^{\frac{1}{2}}+D\bar{z}^{\frac{1}{2}}\overline{\ln(z)}-2D\bar{z}^{\frac{1}{2}}+\frac{C+H}{2}\bar{z}\right]
\end{aligned}
\tag{6}
$$

In the mathematical analysis, the assumption $D + F = 0$ must be made in order to give an appropriate asymptotic behaviour of the stress along the crack flank. Therefore, crack tip displacement fields are defined from the five coefficients: *A*, *B*, *C*, *F* and *H*.

The CJP model provides three stress intensity factors to characterise the stress and displacement fields around the crack tip; an opening mode stress intensity factor K_F, a retardation stress intensity factor K_R, a shear stress intensity factor K_S and also gives the *T*-stress.

The opening mode stress intensity factor K_F is defined using the applied remote load traditionally characterised by K_I but that is modified by force components derived from the stresses acting across the elastic-plastic boundary and which therefore influence the driving force for crack growth. Thus K_F is defined from the asymptotic limit of σ_y as $x \rightarrow +0$, along $y = 0$, i.e. towards the crack tip on the crack plane ahead of the crack tip:

$$
K_F = \lim_{r\to 0}\left[\sqrt{2\pi r}\left(\sigma_y + 2Fr^{-1/2}\ln r\right)\right] = \sqrt{\frac{\pi}{2}}(A-3B-8F) \tag{7}
$$

The retardation stress intensity factor K_R characterises forces applied in the plane of the crack and which provide a retarding effect on fatigue crack growth. Thus, K_R is evaluated from σ_x in the limit as $x \rightarrow$ -0, along $y = 0$, i.e. towards the crack tip along the crack flank:

$$K_R = \lim_{r \to 0} \left[\sqrt{2\pi r}\, \sigma_x \right] = -(2\pi)^{3/2} F \tag{8}$$

It is proposed in the CJP model that a shear term arises from the requirement of compatibility of displacements between the bulk elastic region (Poisson's ratio 0.3) and the plastic zone (Poisson's ration 0.5). The mathematical analysis produces a *ln* term, which has the same form as the stress field terms associated with dislocations. Riemelmoser and Pippan [13] proposed a dislocation model for plasticity-induced closure in plane strain and this produces a shear stress from elastic rotation of the lattice in the plastic wake. This effect is the same basic compatibility concept that the original CJP assumptions use in generating the stress terms. A shear stress intensity factor K_S therefore characterises compatibility-induced shear stress along the plane of the crack at the interface between the plastic enclave and the surrounding elastic field and is derived from the asymptotic limit of σ_{xy} as $x \rightarrow$ -0, along $y = 0$, i.e. towards the crack tip along the crack wake:

$$K_S = \lim_{r \to 0} \left[\sqrt{2\pi r}\, \sigma_{xy} \right] = \mp \sqrt{\frac{\pi}{2}} (A + B) \tag{9}$$

A positive sign indicates y > 0, and a negative sign that y < 0.

The *T*-stress, which is found as components T_x in the *x*-direction and T_y in the *y*-direction is given by:

$$\begin{aligned} T_x &= -C \\ T_y &= -H \end{aligned} \tag{10}$$

The correspondence between crack tip stress and displacement fields is explored later in this paper as part of the validation of the method.

These new stress intensity factors are somewhat controversial, so the present paper is primarily orientated towards demonstrating the capability of the CJP model to provide improved predictions of the plastic zone size and shape associated with a growing fatigue crack.

2. Experimental work

Two compact tension (CT) specimens (dimensions given in Figure 2) were manufactured from a 1 mm thick sheet of commercially pure Grade 2 titanium and subjected to constant amplitude fatigue loading using two different values of *R*-ratio (0.6 and 0.1) whilst maintaining a constant

value of maximum load (750 N) in the fatigue cycle. Tables 1 and 2 present typical chemical analysis and mechanical property data for this CP titanium alloy.

The two faces of each specimen were prepared for experimental observations in two different ways. The surface to be used for digital image correlation (DIC) was treated by spraying a black speckle with an airbrush over a white background, while the other face was polished to assist in tracking the crack tip with a zoom lens.

Fatigue tests were conducted on an ElectroPuls E3000 electrodynamic machine (Figure 3) at a frequency of 10 Hz. A CCD camera fitted with a macro-zoom lens (MLH-10X EO) to increase the spatial resolution at the region around the crack tip, was placed perpendicular to each face of the specimen. During fatigue testing, the cycling was periodically paused to allow acquisition of a sequence of images at uniform increments through a complete loading and unloading cycle. The CCD camera viewing the speckled face of the specimen was set up so that the field of view was 17.3 x 13 mm (resolution of 13.5 μm/pix) with the crack path located at the centre of the image. Illumination of the surface was provided by a fibre optic ring placed around the zoom lens (also shown in Figure 3). Figure 4 shows a typical example of both the horizontal and vertical displacement field data obtained at a crack length of 9.40 mm under an applied load of 750 N.

3. Experimental methodology

This section outlines the two methodologies developed to evaluate the plastic zone size and shape. The first technique is a direct method in which the plastic zone is estimated from the displacement fields determined by experiment; while the second one is an indirect method in which data from experiments is employed in the models to determine the plastic zone size and shape. These two methods are described in the following sections.

3.1. Direct experimental method for estimating the plastic zone

This method is based on the application of a yield criterion and consists of identifying the plastic stress field by differentiating the experimentally measured displacement fields. In this work, 2D-DIC has been employed to make experimental displacement measurements; however, any technique that allows the crack tip displacement fields to be obtained would be applicable. The procedure for implementing this method is described in the following paragraphs.

The authors note that truncation of the stress distribution above the elastic yield point will lead to a redistribution of the stress field and an increase in size of the plastic zone (e.g. the so-called Irwin plastic zone correction to crack length concept). The interest in this paper, however, is in comparing three elastic crack tip stress field models in terms of their ability to characterise the shape and size of the plastic zone solely on the basis of the underlying free-body diagram

assumptions, rather than including derived second order corrections in the analysis. Thus the authors have explicitly avoided considering plastic zones in detail, preferring to take a similar elastic stress approach to that originally used by Irwin. The CJP model is, however, 'improved' compared with the Irwin model by the incorporation of the elastic stresses generated at the boundary of the plastic zone by its existence, and which are believed to act on the applied elastic stress field. Thus a comparison with the Williams and Westergaard models is fair as all three models are elastic stress models. The authors believe that the continuing benefit of the elastic stress intensity factor approach derives from the defocusing on the details of the plastic zone and that a more refined model is capable of better dealing with crack tip shielding.

The first step in the methodology consists in obtaining the horizontal and vertical displacement fields around the crack tip. Typical examples of displacement maps were shown in Figure 4 for a crack length of 9.40 mm and a load level of 750 N and the process will be illustrated using these displacement maps. The next step in the process involves determining the strain fields at the crack tip by differentiation of the displacement fields. For this purpose, the Green-Lagrange strain tensor [14] is employed because it considers the second order terms and is more accurate than those using only first order terms. Thus, this strain tensor is given by the following expressions:

$$\begin{pmatrix} \varepsilon_{xx} \\ \varepsilon_{yy} \\ \varepsilon_{xy} \end{pmatrix} = \begin{pmatrix} \dfrac{\partial u}{\partial x} \\ \dfrac{\partial v}{\partial y} \\ \dfrac{\partial u}{\partial y} + \dfrac{\partial v}{\partial x} \end{pmatrix} + \frac{1}{2} \begin{pmatrix} \dfrac{\partial u}{\partial x} & 0 & \dfrac{\partial v}{\partial y} & 0 \\ 0 & \dfrac{\partial u}{\partial y} & 0 & \dfrac{\partial v}{\partial y} \\ \dfrac{\partial u}{\partial y} & \dfrac{\partial u}{\partial x} & \dfrac{\partial v}{\partial y} & \dfrac{\partial v}{\partial x} \end{pmatrix} \begin{pmatrix} \dfrac{\partial u}{\partial x} \\ \dfrac{\partial u}{\partial y} \\ \dfrac{\partial v}{\partial x} \\ \dfrac{\partial v}{\partial y} \end{pmatrix} \tag{11}$$

Once the strain fields have been calculated, the next step is to determine the stress fields using Hooke's law. The equivalent stress is calculated from the stress tensor either using the second invariant of the stress deviator (von Mises), or the difference of the maximum and minimum principal stress (Tresca). An estimate of the size and shape of the plastic zone is obtained by connecting all points where the yield criterion is met, i.e., where the equivalent stress is equal to the yield stress. Figures 5a and 5b show the region of equivalent stress where the value exceeds the yield stress for both the von Mises and Tresca yield criteria. Thus, the plastic zone area (white) can be easily identified from the surrounding elastic field.

In this paper, the area of the plastic zone has been considered as a variable that contains information on both size and shape and which can therefore provide an efficient and powerful technique for making quantitative measurements. Once the plastic zone has been identified, the next step is to characterise its size by quantifying its area at the crack tip. Initially, a set of data

points that define the equivalent yield stress contour of the plastic zone must be detected (Figure 5c). Next, a triangulation function is applied to define the area enclosed by these data points (Figure 5d). Finally, the plastic zone area can be calculated as the sum of the areas of all the triangles previously defined in the triangulation process.

3.2. Indirect method for estimating the plastic zone

The plastic zone area calculated from experimental data will be compared with theoretical analytical predictions in order to validate the proposed methodology. The method used here takes the three crack tip stress models considered in this paper (Williams, Westergaard and CJP) to infer plastic zone shapes that can then be compared with the experimentally derived value.

In the literature, the two most popular methods used to estimate the plastic zone size are the Irwin and Dugdale approaches. Both approaches lead to simple estimates for crack tip plastic zone size based on elastic solutions, although the assumed plastic zone shape does not agree with those experimentally observed in metals [15]. It is more useful to estimate the size and shape of the plastic zone at all angles around the crack tip by applying a yielding criterion to an analytical model [1, 9, 10, 16] that describes the crack tip stress field. In this work, the three models described in section 2 were used to find the plastic zone shape.

The first step in such an analysis consists in determining the stress intensity factors in each crack tip stress model from analysis of the experimental displacement fields. The multi-point over-deterministic method developed by Sanford and Dally [17] forms the basis for this process. The models are valid only for the elastic field near the crack tip singularity and hence it was necessary to identify the near-tip zone where valid experimental data could be obtained. An annular mesh was therefore defined, as indicated in Figure 6, on the basis of inner and outer radii. The inner radius was defined with sufficient extent to avoid including plastic deformation at the crack tip, while the outer radius was defined from the singularity dominated zone. The accuracy of location of the crack tip position is important, and this was taken into account through the quality of the mathematical fit via the statistical parameters of the mean and the variance. Thus, the solution was found using the lowest values of the mean and the variance as a function of the crack tip coordinates. The region of data collection does not encompass the crack flanks to avoid collecting data where the elastic crack tip stress field no longer describes the state of stress.

The vertical displacement maps were used to identify this singularity dominated region (region marked in Figure 4b) via the assumption that the point where crack tip displacement fringes became straight and perpendicular to the crack was where the influence of the singularity ceased to dominate. Once the stress intensity factors have been calculated, the next step in the method entails evaluating the crack tip stress fields using these coefficients. From this point on, the

procedure is similar to that described in section 3.1 for the direct method. Hence the size and shape of the experimentally determined plastic zone can be compared with that found using the three different theoretical models that describe the crack tip stress and displacement fields.

4. Results and discussion

Figure 7 shows size and shape data obtained for the plastic zone at maximum load using the von Mises yield criterion for the specimen tested at $R = 0.6$ at four different crack lengths (6.42, 7.26, 8.13 and 9.20 mm). The white area represents the experimental plastic zone estimated from the direct method, while the dotted contours correspond to the plastic zone found for the three models by implementing the indirect method using the model coefficients. It is clear that the plastic zone size and shape predicted by the CJP model is an excellent fit to the experimental data, while the Westergaard and Williams models predict somewhat larger dimensions.

Figure 8 shows the evolution of both experimental and predicted plastic zone area with the crack length for a test conducted at $R = 0.6$ using the von Mises yield criterion. Again, the experimental data is in close agreement with the plastic zone area calculated from the CJP model at all crack lengths, while the predicted area using the Westergaard and Williams models is higher than the experimental results. The Westergaard model shows a progressively larger error as the crack length increases while the error in the Williams solution remains fairly constant. It can be concluded that the CJP model provides an improved prediction of the crack tip plastic zone area and shape compared with either the Westergaard or Williams models.

Figure 9 illustrates the difference that choice of yield criterion (von Mises or Tresca) would make to the experimental and CJP predictions of plastic zone area. As expected, sizes predicted using the Tresca criterion are higher, but close agreement is still observed between the experimental predictions and those provided by the CJP model. In absolute terms, the differences between the values seems quite small, but the authors believe that in terms of the dimensions of the specimens and the low values obtained for the plastic zone area, these are significant differences in terms of accuracy of the underlying models.

All results discussed so far correspond to the specimen tested at the higher value of $R = 0.6$. However, the evolution of the plastic zone area at low R-ratio has been investigated also employing both, the direct and indirect methods, and implementing the von Mises yield criterion. Figure 10 compares the experimental and CJP model predictions of plastic zone area for the high R (CT1) and low R (CT2) specimens. It can be seen that the plastic zone area obtained for the specimen tested at low R-ratio is smaller than the estimated value for the specimen tested at high R-ratio. This is thought to be a consequence of the cyclic plastic zone generated at the crack tip by the applied fatigue cycle, which is a result of the compressive residual stresses introduced during load cycling [18]. The cyclic plastic zone would be larger in

the case of the specimen tested at low R-ratio because the applied load range is higher and hence has a greater influence on compressive residual stresses.

The interpretation of these observations is that reverse plasticity influences plasticity-induced crack shielding in the case of the specimen tested at R = 0.1. This can be further explored by considering the data from the CJP model for K_F, K_R and K_S obtained during a loading half-cycle at the longest crack length in each specimen, CT1 (R = 0.6, a = 9.20 mm) and CT2 (R = 0.1, a = 9.40 mm) (Figure 11). In the specimen tested at high R-ratio (Figure 11a) the K_F values closely follow the trend in the nominal K_I values. In contrast, in the case of the specimen tested at low R-ratio, K_F deviates above the nominal K_I once the values fall below approximately 15 MPa·m$^{1/2}$, which corresponds to a load level of 250 N. This behaviour is similar to that reported by Elber [19, 20] when he originally defined plasticity-induced crack closure. He noticed an anomaly in the elastic compliance of fatigue specimens, where at high loads the measured compliance agreed with that obtained from standard expressions for fracture mechanics specimens, whilst at low loads the compliance was close to that for an uncracked specimen. Elber attributed this change in compliance to contact between crack surfaces (i.e., crack closure) in the lower part of the load cycle as a consequence of the residual tensile plastic deformation left in the wake of a fatigue crack tip. The present authors believe that wake contact is only one of several possible mechanisms that lead to plasticity-induced crack tip shielding, with the compatibility induced stresses at the elastic-plastic boundary contributing a further component. The net effect of the shielding mechanisms is represented in the CJP model by the terms K_R and K_S.

In Figure 11b, K_R and K_S have been plotted as a function of the applied nominal K_I. For the specimen tested at R = 0.1 (CT2), and starting from the maximum nominal applied stress intensity factor, K_R increases gradually until approximately 15 MPa·m$^{1/2}$ (250 N), where there is a sudden sharp increase in its value. This behaviour makes sense in terms of the definition of K_R as a retarding stress intensity factor, since below 250 N crack surface contact is likely to occur due to the action of the surrounding elastic field on the plastic enclave. Hence there is a relationship between the behaviour of K_F and K_R. In the case of the specimen tested at R = 0.6 there is no sharp change in the trend of K_R values throughout the complete loading cycle.

At R = 0.1 the K_S values (Figure 11b) appear initially to remain constant and slightly negative corresponding to the portion of the load cycle below approximately 15 MPa·m$^{1/2}$ and then gradually become more negative. Again, this behaviour is reasonable because K_S is characterised by an interfacial shear force at the elastic-plastic boundary and its effect is probably insignificant at low loads whilst the crack surfaces are in contact, and has a greater influence as the applied load increases beyond 15 MPa·m$^{1/2}$.

This analysis of the trends in the three stress intensity factors defined in the CJP model indicates that it is possible to identify the portion of the load cycle where there is a plasticity-induced shielding effect on the elastic crack tip field ahead of the crack tip.

5. Conclusions

In the present paper a novel experimental methodology for the quantitative evaluation of the crack tip plastic zone size during fatigue crack growth has been presented. This methodology uses differentiation of the measured displacement fields to obtain strain maps that can be combined with a yield criterion to estimate the shape and size of the crack tip plastic zone. These predictions can be compared with estimates of the plastic zone size obtained from analytical models that describe crack tip displacement fields. This work indicates that the CJP model provides the best prediction of the crack tip plastic zone shape and size. It is proposed that this agreement supports the fact that the CJP model, through its basic assumptions regarding the influences of plasticity on the elastic stress fields ahead of the crack tip, is better at defining the real size of the plastic zone. The CJP model was constructed on the basis of capturing the elastic stresses at the elastic-plastic boundary arising from the total plastic enclave around the crack, as well as arising from the imposed elastic stress field. It therefore explicitly incorporates terms arising from the residual stresses which are caused by fatigue crack growth. If the underlying assumptions of these influences are correct then one would expect a better characterisation of the experimental plastic zone size and shape than would be found with the Williams or Westergaard models. In addition, the influence of the R-ratio on the size of the plastic zone has been also investigated via fatigue tests at R=0.1 and R=0.6. The plastic zone area was smaller at the lower R-ratio, which can be associated to plasticity induced shielding during fatigue crack growth. To support this hypothesis the CJP model has been employed to calculate and evaluate the stress intensity factors during a loading cycle. It is clearly observed that at the lower R-ratio a change in the observed trend occurs compared to the higher. From this analysis it has been possible to estimate in which portion of the cycle the crack is open or close.

Results presented in the current paper are intended to contribute to a better understanding of the shielding effects of crack tip plasticity during fatigue crack growth. The CJP model has been demonstrated to be a valuable tool in the study of crack tip plasticity and plasticity-induced shielding.

References

[1] M.N. James, C.J. Christopher, Y. Lu, E.A. Patterson, Local crack plasticity and its influences on the global elastic stress field, International Journal of Fatigue, 46 (2013) 4-15.

[2] Uğuz, J.W. Martin, Plastic zone size measurement techniques for metallic materials, Materials Characterization, 37 (1996) 105-118.

[3] A. Steuwer, L. Edwards, S. Pratihar, S. Ganguly, M. Peel, M.E. Fitzpatrick, T.J. Marrow, P.J. Withers, I. Sinclair, K.D. Singh, N. Gao, T. Buslaps, J.Y. Buffière, In situ analysis of cracks in structural materials using synchrotron X-ray tomography and diffraction, Nuclear Instruments and Methods in Physics Research Section B: Beam Interactions with Materials and Atoms, 246 (2006) 217-225.

[4] D. Nowell, P.F.P. de Matos, Application of digital image correlation to the investigation of crack closure following overloads, Procedia Engineering, 2 (2010) 1035-1043.

[5] F. Díaz, Some improvements in the analysis of fatigue cracks using thermoelasticity, International Journal of Fatigue, 26 (2004) 365-376.

[6] S.I. Wright, M.M. Nowell, D.P. Field, A review of strain analysis using electron backscattter diffraction, Microscopy and Microanalysis, 17 (2011) 316-329.

[7] C. Roux-Langlois, A. Gravouil, M.C. Baietto, J. Réthoré, F. Mathieu, F. Hild, S. Roux, DIC identification and X-FEM simulation of fatigue crack growth based on the Williams' series, International Journal of Solids and Structures, 53 (2015) 38-47.

[8] C.J. Christopher, G. Laboviciute, M.N. James, E.A. Patterson, Extension of the CJP model to mixed mode I and mode II, Frattura ed Integrita Strutturale, 7 (2013) 161-166.

[9] M. Janssen, J. Zuidema, R.J.H. Wanhill, Fracture Mechanics, 2nd Edition, Spon Press, Abingdon, 2006.

[10] K. Ramesh, S. Gupta, A.A. Kelkar, Evaluation of stress field parameters in fracture mechanics by photoelasticity—Revisited, Engineering Fracture Mechanics, 56 (1997) 25-45.

[11] J.R. Yates, M. Zanganeh, Y.H. Tai, Quantifying crack tip displacement fields with DIC, Engineering Fracture Mechanics, 77 (2010) 2063-2076.

[12] N.I. Muskhelishvili, Some Basic Problems of the Mathematical Theory of Elasticity, Noordhoff International Publishing, Groningen, 1977.

[13] F.O. Riemelmoser and R. Pippan, Mechanical reasons fro plasticity-induced crack closure under plane strain conditions, Fatigue and Fracture of Engineering Materials and Structures, 21 (1998) 1425-1433.

[14] A.K. Singh, Mechanics of Solids, Prentice-Hall of India, 2010.

[15] T.L. Anderson, Fracture Mechanics: Fundamentals and applications, 3th edition, CRC Press LLC, Boca Raton, USA, 2005.

[16] A.D. Nurse, E.A. Patterson, Determination of predominantly mode II stress intensity factors from isochromatic data, Fatigue and Fracture of Engineering Materials and Structures, 16 (1993) 1339-1354.

[17] R.J. Sanford, J.W. Dally, A general method for determining mixed-mode stress intensity factors from isochromatic fringe patterns, Engineering Fracture Mechanics, 11 (1979) 621-633.

[18] J.R. Rice, Mechanics of crack-tip deformation and extension by fatigue, in: J. Grosskreutz (Ed.) STP 415 Fatigue Crack Growth, ASTM, PA, USA, 1967.

[19] W. Elber, Fatigue crack closure under cyclic tension, Engineering Fracture Mechanics, 2 (1970) 37-45.

[20] W. Elber, The significance of fatigue crack closure, in: M.S. Rosenfeld (Ed.) STP 486 Damage Tolerance in Aircraft Structures, ASTM, PA, USA, 1971.

Tables

Table 1 Chemical composition for commercially pure titanium grade 2.

Element	Nitrogen	Carbon	Hydrogen	Iron	Oxygen	Titanium
Spec. wt%	≤0.05	≤0.08	≤0.015	<0.20	≤0.20	balance
Actual wt%	<0.01	0.01	0.002	0.10	0.12	balance

Table 2 Mechanical properties for the commercially pure titanium used in this work.

Mechanical property	**Unit**	**Value**
Young's modulus	MPa	105,000
Yield stress	MPa	390
Ultimate stress	MPa	448
Elongation	%	20
Poisson's ratio	-	0.33

Figures

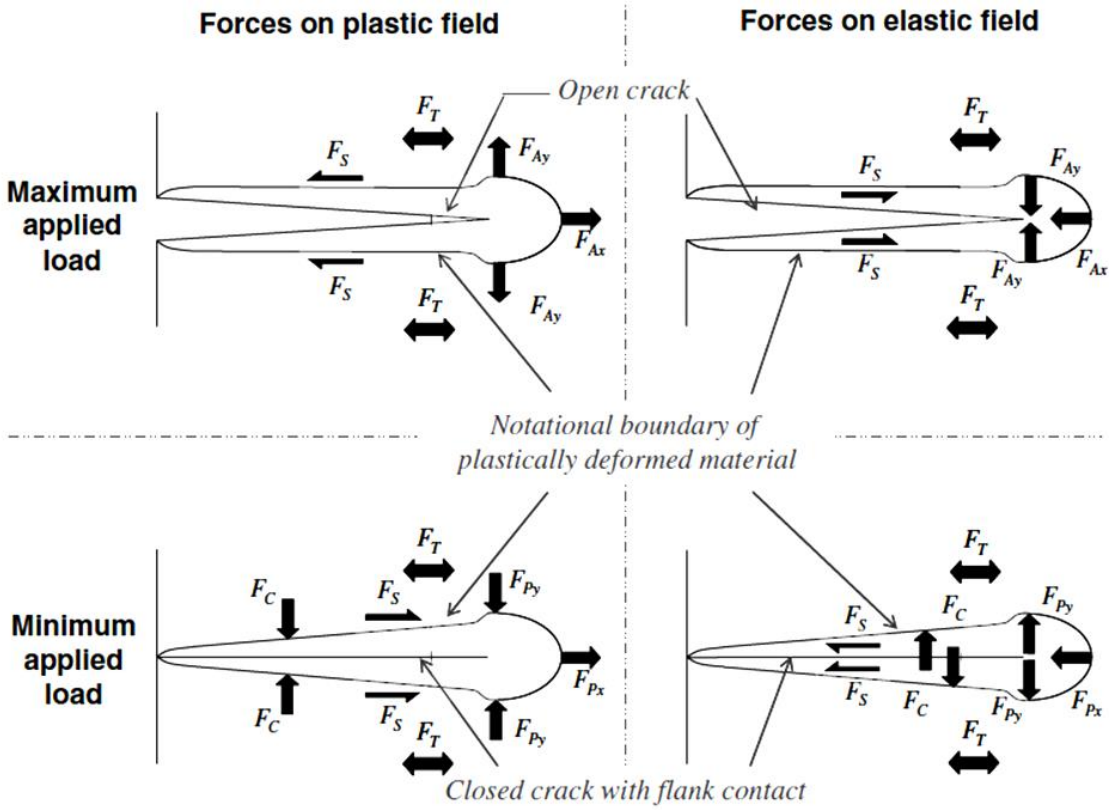

Figure 1 Free-body diagram illustrating the forces acting at the interface of the plastic zone and the surrounding elastic material [1].

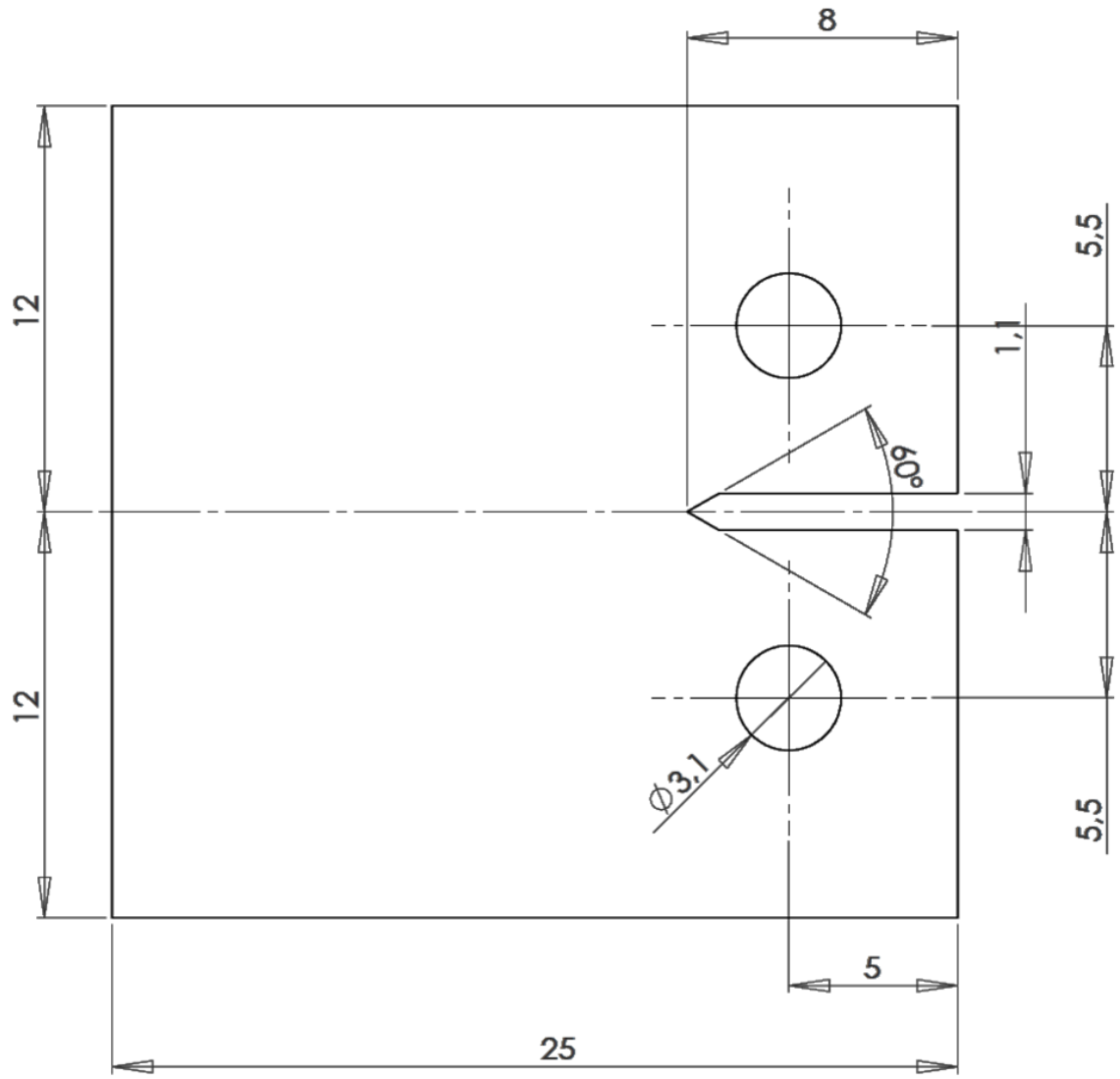

Figure 2 Geometry and dimensions (mm) of the titanium compact tension specimens used in this work.

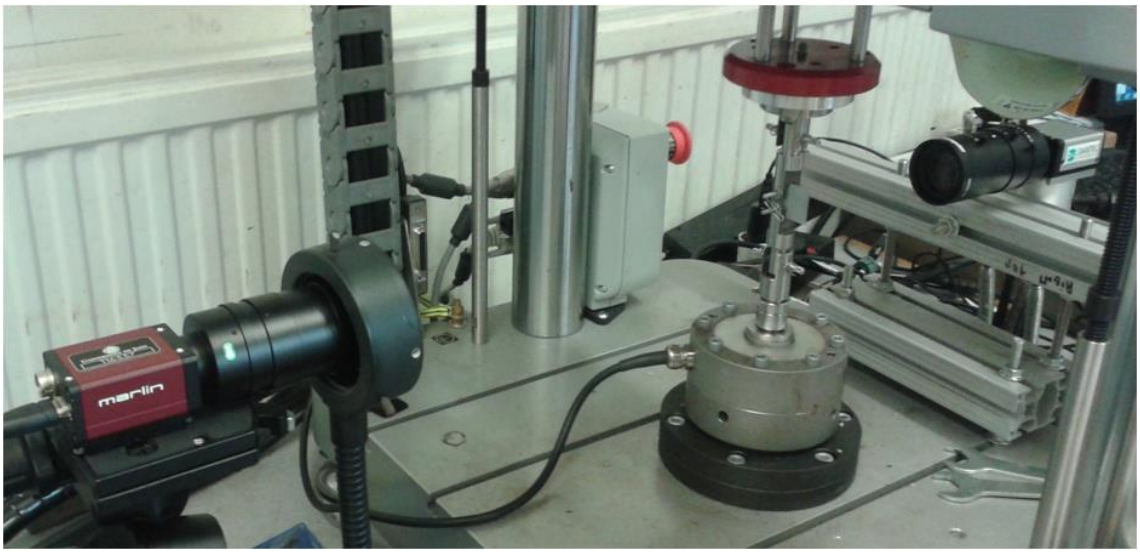

Figure 3 Experimental setup used to measure DIC data during fatigue testing.

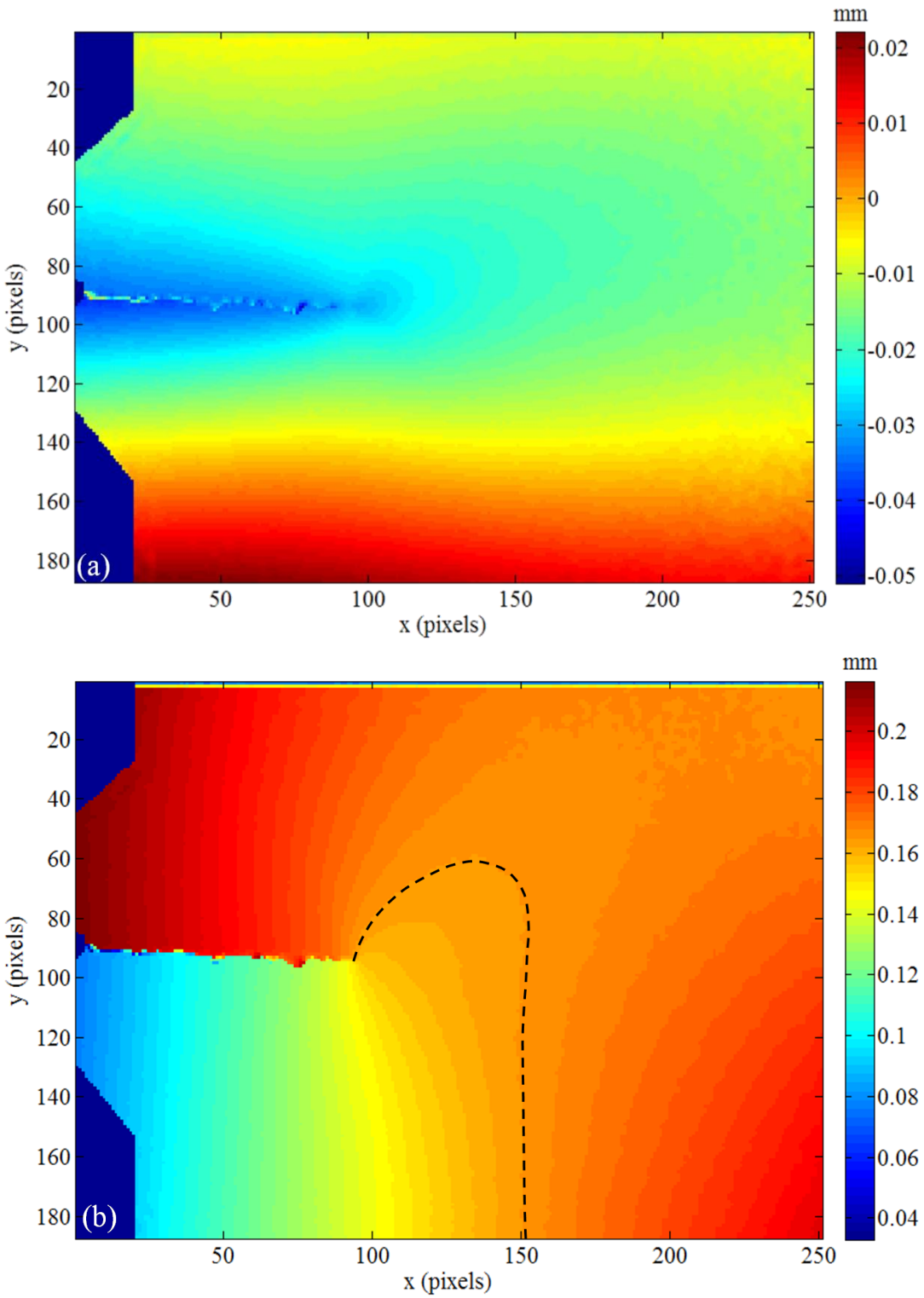

Figure 4 DIC images showing the measured displacement fields at the crack tip for a crack length of 9.40 mm and a load level of 750 N. (a) Horizontal and (b) vertical displacement fields. The boundary between the area dominated by the crack tip and that dominated by the free edge of the specimen is marked with the black dashed line.

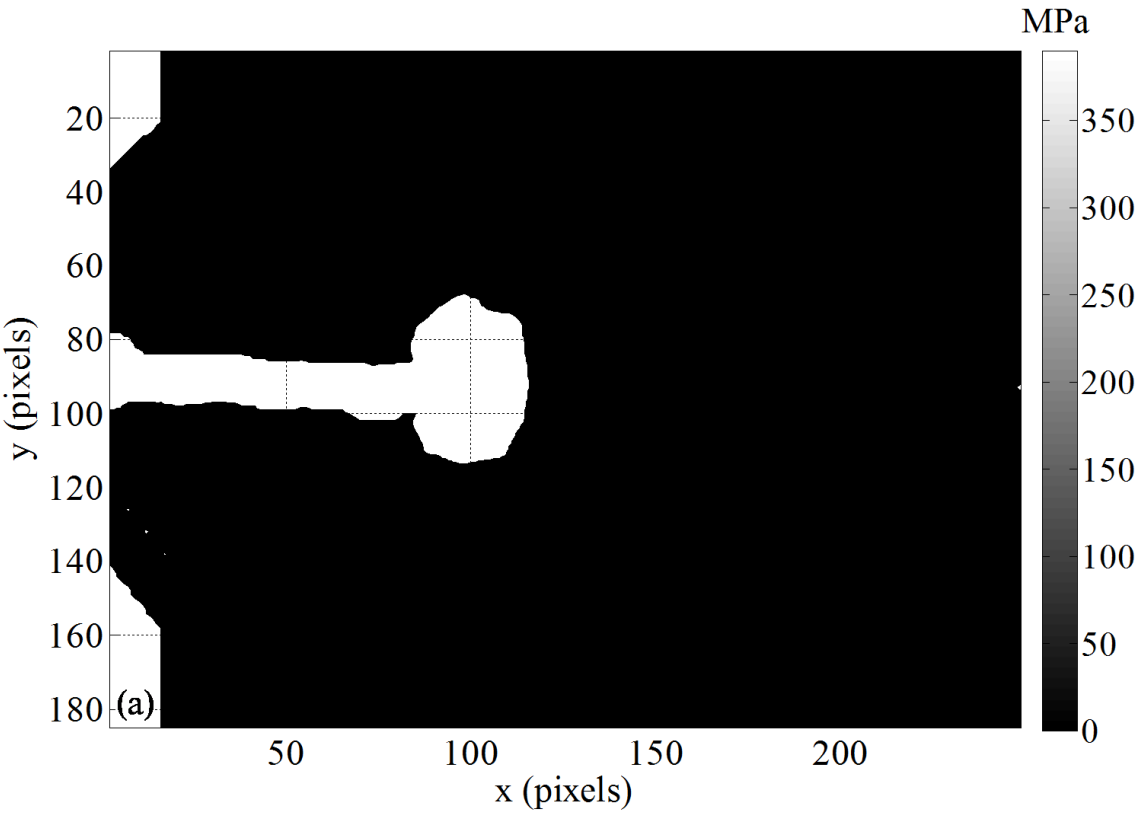
MPa
350
300
250
200
150
100
50
0
20
40
60
80
100
120
140
160
180
y (pixels)
50
100
150
200
x (pixels)
(a)

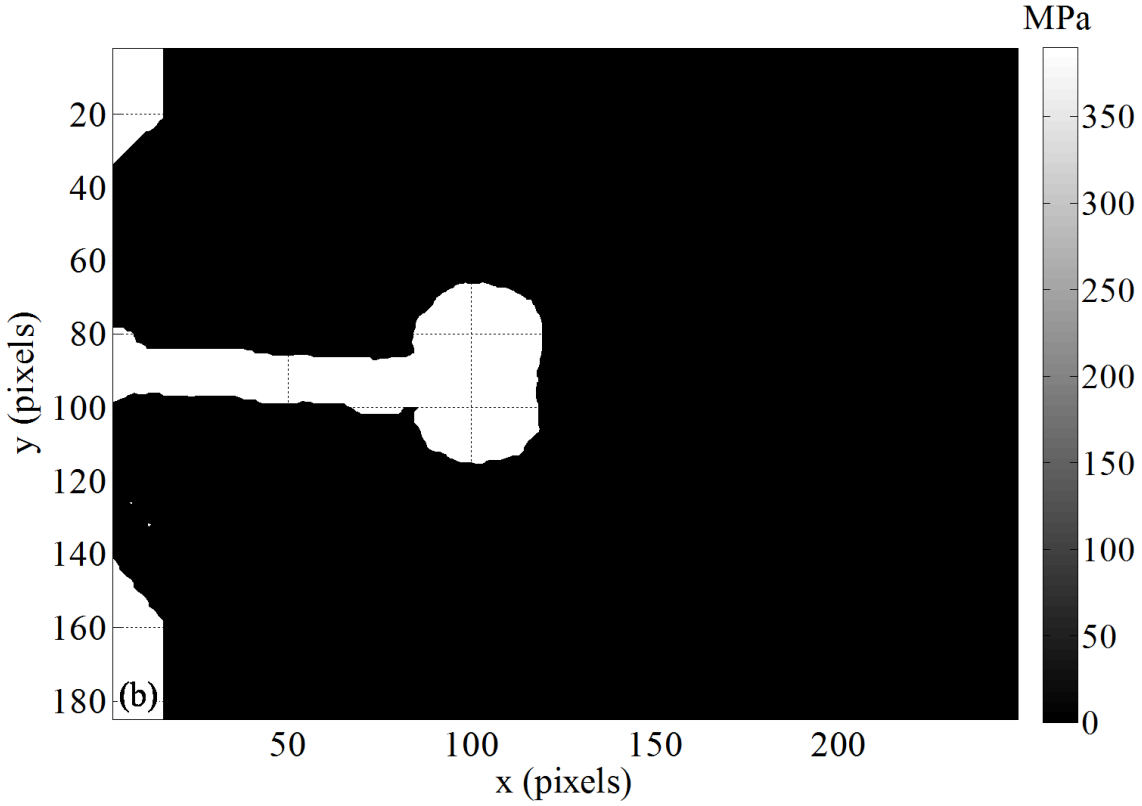
MPa
350
300
250
200
150
100
50
0
20
40
60
80
100
120
140
160
180
y (pixels)
50
100
150
200
x (pixels)
(b)

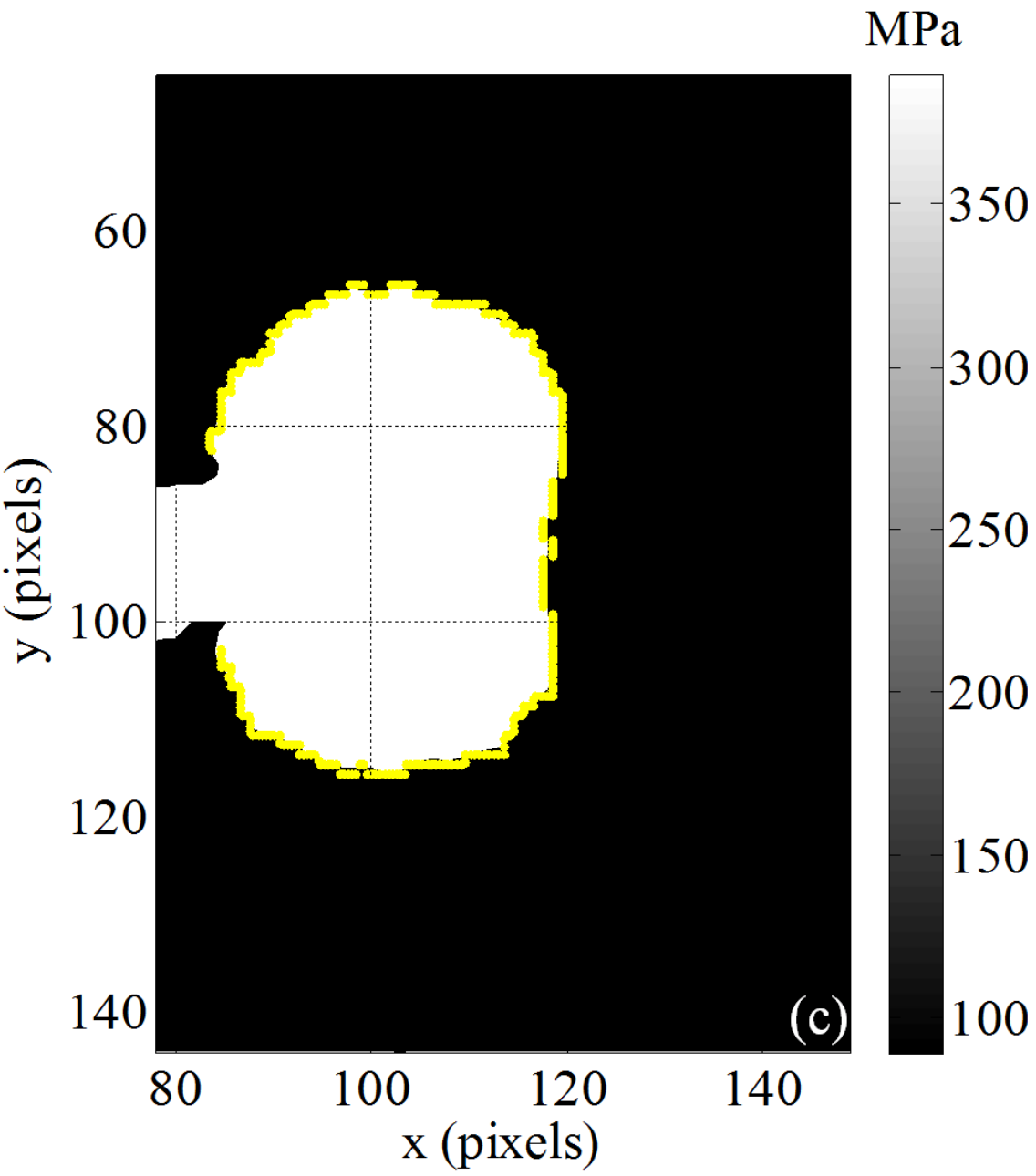
MPa
350
300
250
200
150
100
60
80
100
120
140
y (pixels)
80
100
120
140
x (pixels)
(c)

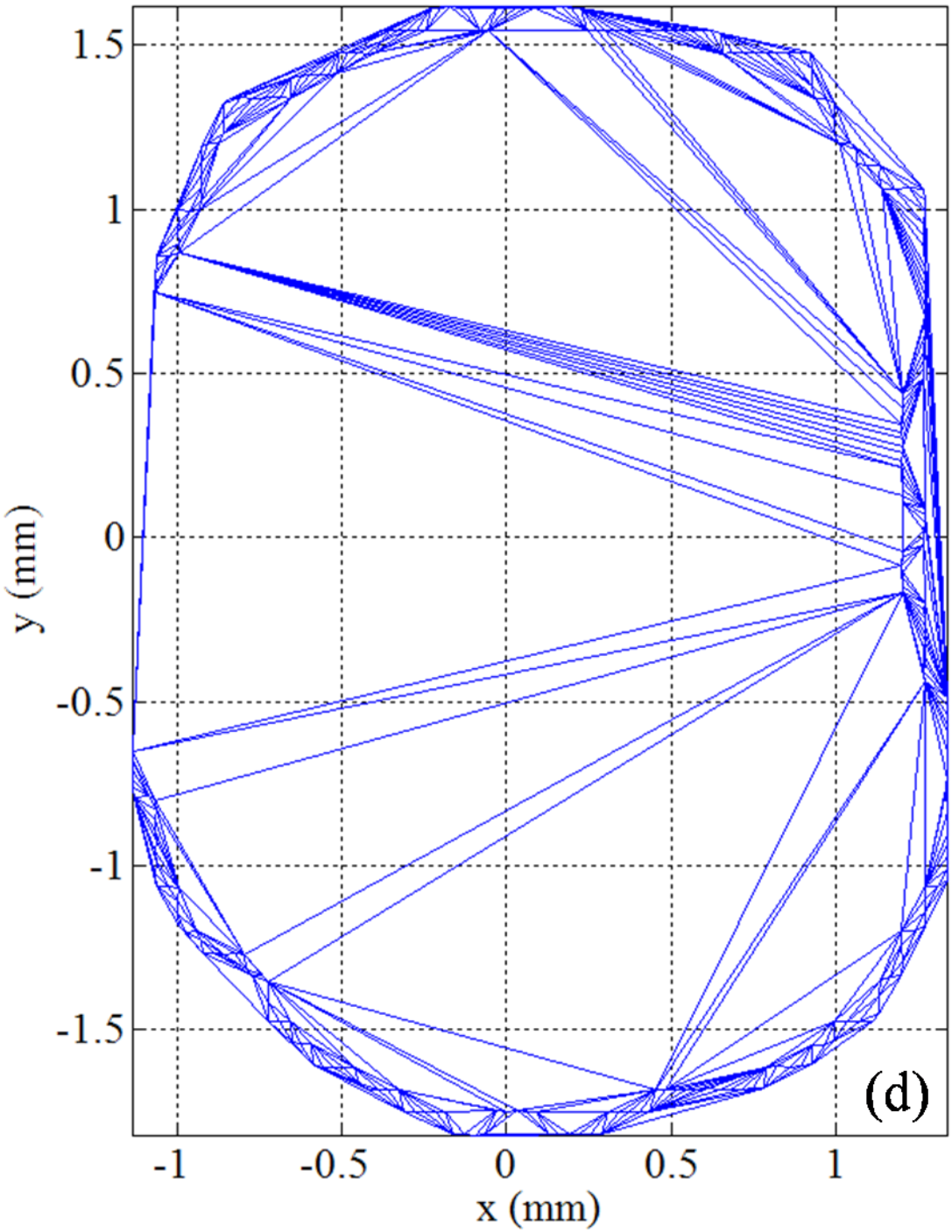

Figure 5 Illustrations showing the equivalent stress maps above the yield stress corresponding to von Mises (a) and Tresca (b) criteria by the yield stress value for a 9.40 mm crack length at a load level of 750 N, and the triangulation process used to calculate the plastic zone area: (c) Detection of the data points defining the equivalent yield stress contour of the plastic zone and (d) triangulation of the enclosed area for calculation purposes (A = 7.58 mm^2).

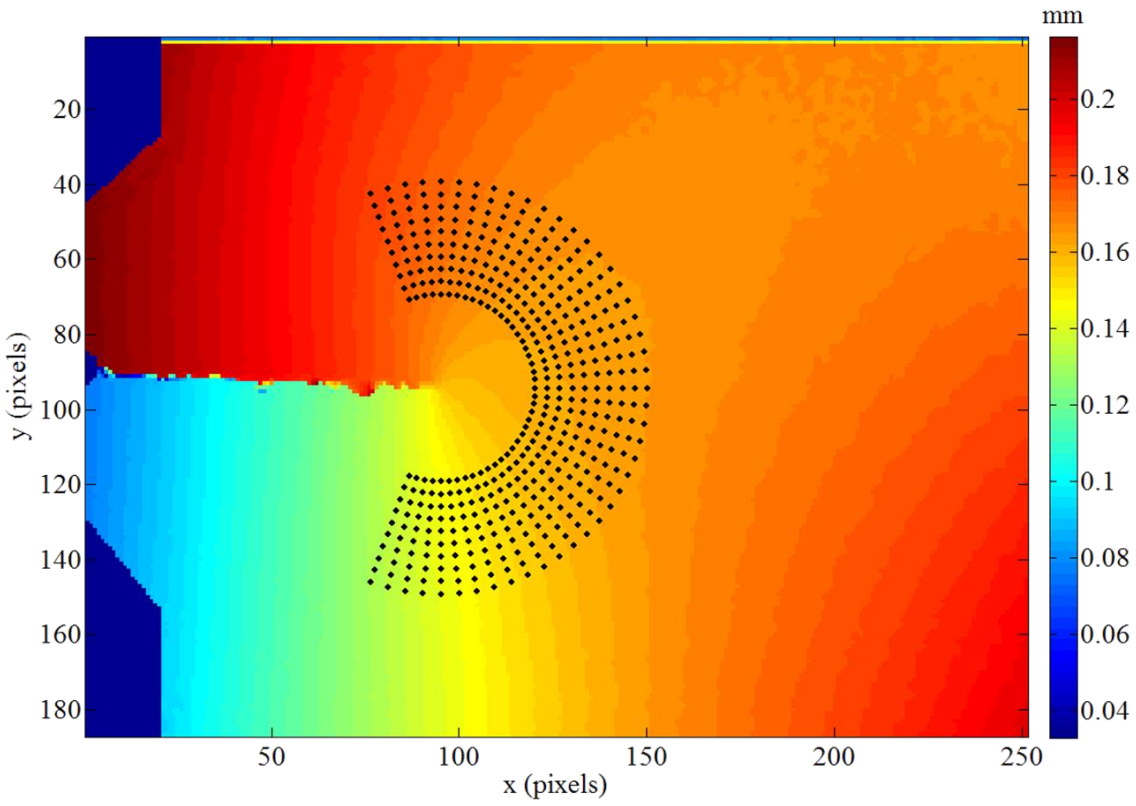

Figure 6 The circular mesh of data points used to define the near-tip region of valid DIC data used in the calculation of stress intensity factors.

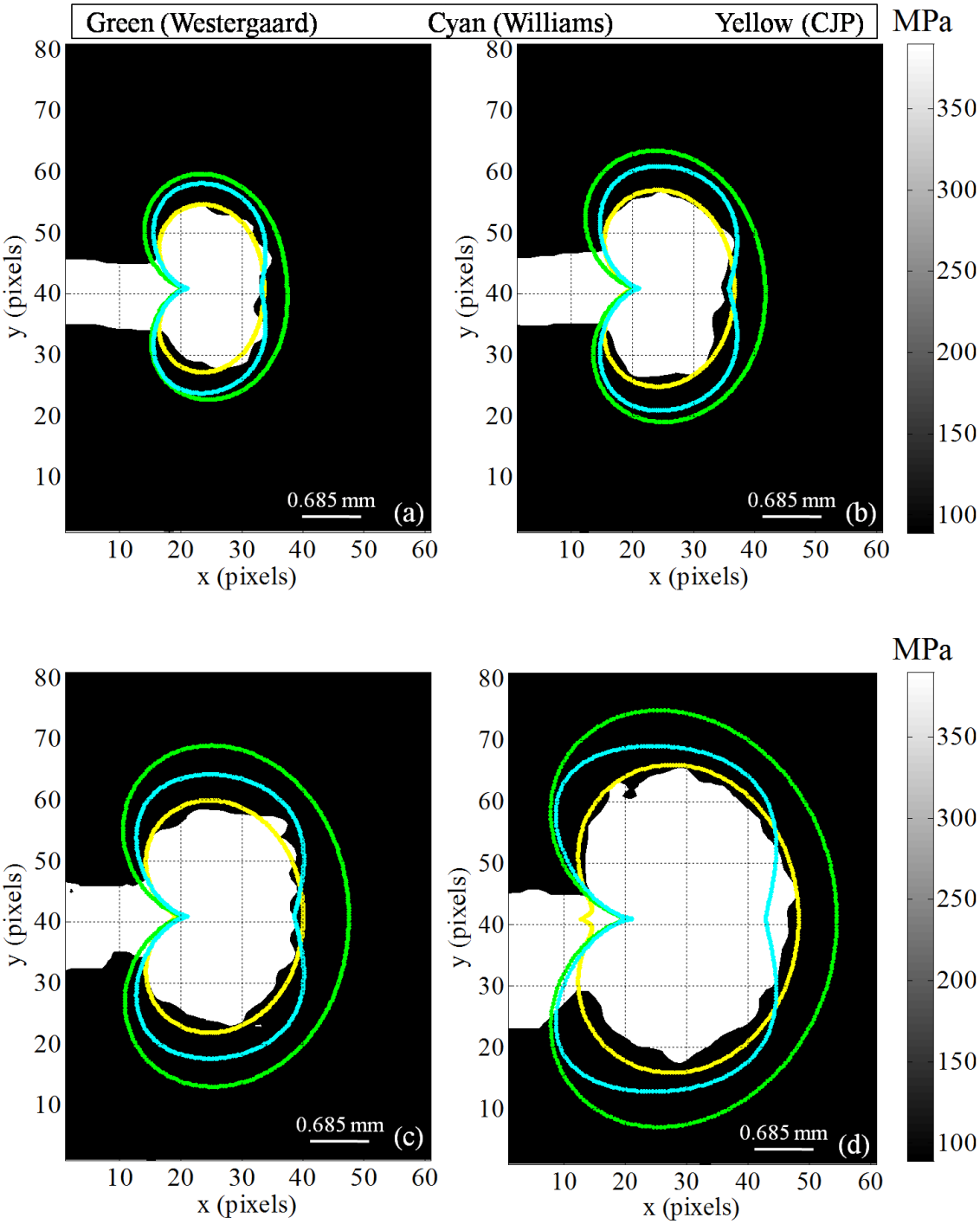

Figure 7 Comparison between the experimental and theoretical plastic zone shapes obtained using the von Mises yield criterion at maximum load and R = 0.6 for four different crack lengths (6.42, 7.26, 8.13 and 9.20 mm). The experimental plastic zone is the white area while the contour lines represent the three analytical models (Westergaard – green; Willliams – cyan and CJP – yellow).

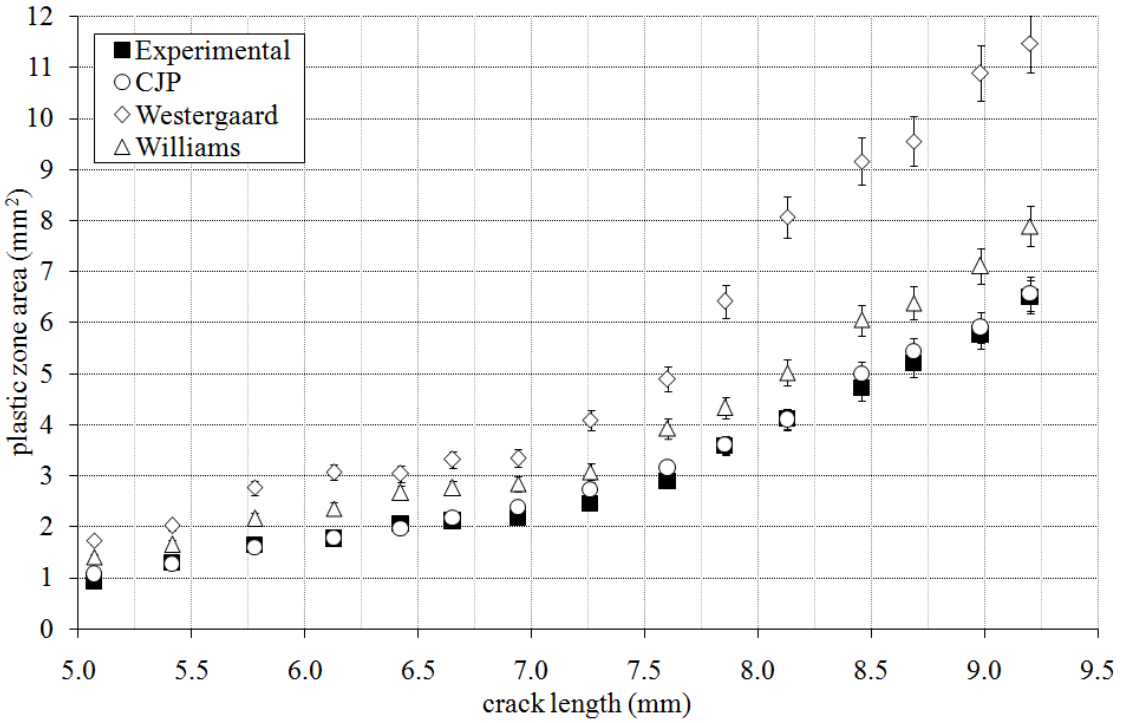

Figure 8 Comparison between the experimental and model predictions of plastic zone area at maximum applied load and R = 0.6 as a function of crack length, using the von Mises yield criterion.

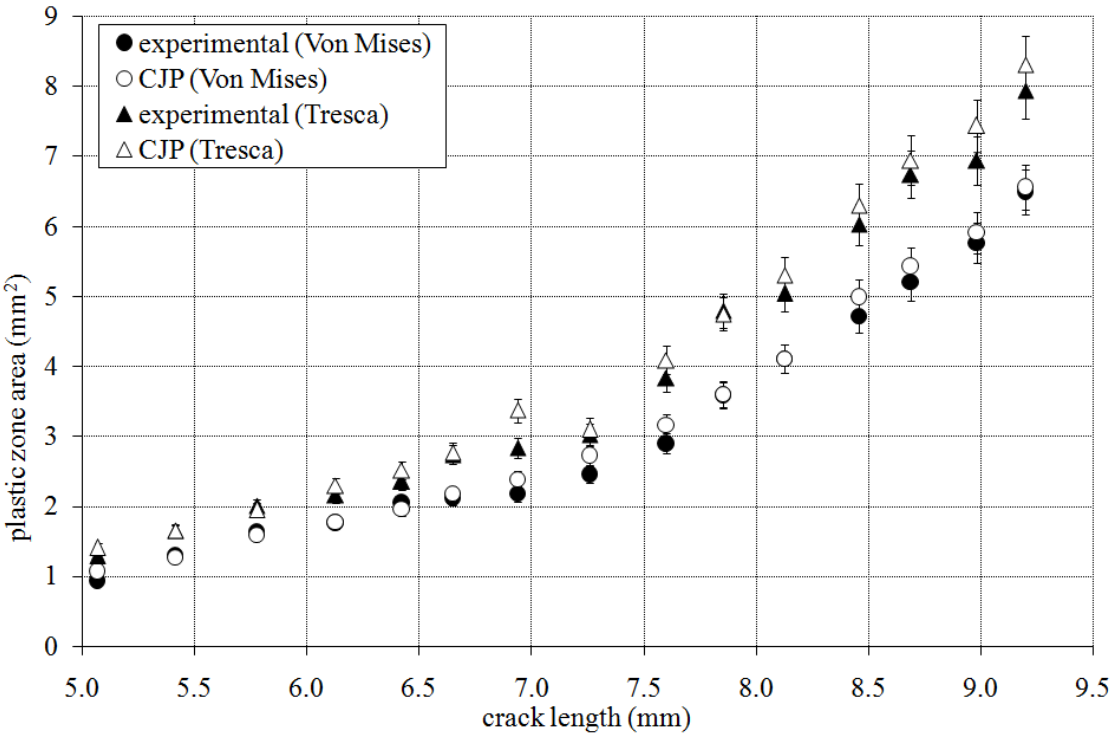

Figure 9 Comparison between the experimental and CJP model predictions of plastic zone size at maximum load and R = 0.6 using both the von Mises and Tresca yield criteria. Good agreement can be observed in both cases.

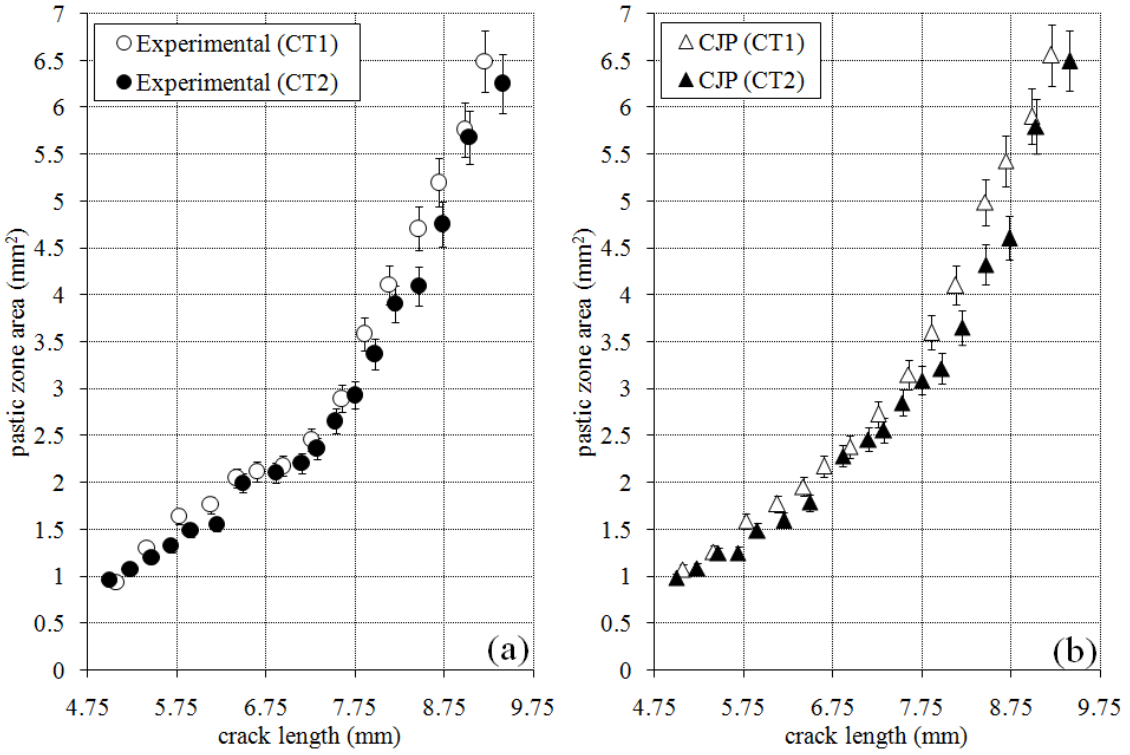

Figure 10 Comparison between the experimental and CJP predictions of plastic zone area as a function of crack length at maximum load for R = 0.6 (CT1) and R = 0.1 (CT2), using the von Mises yield criterion.

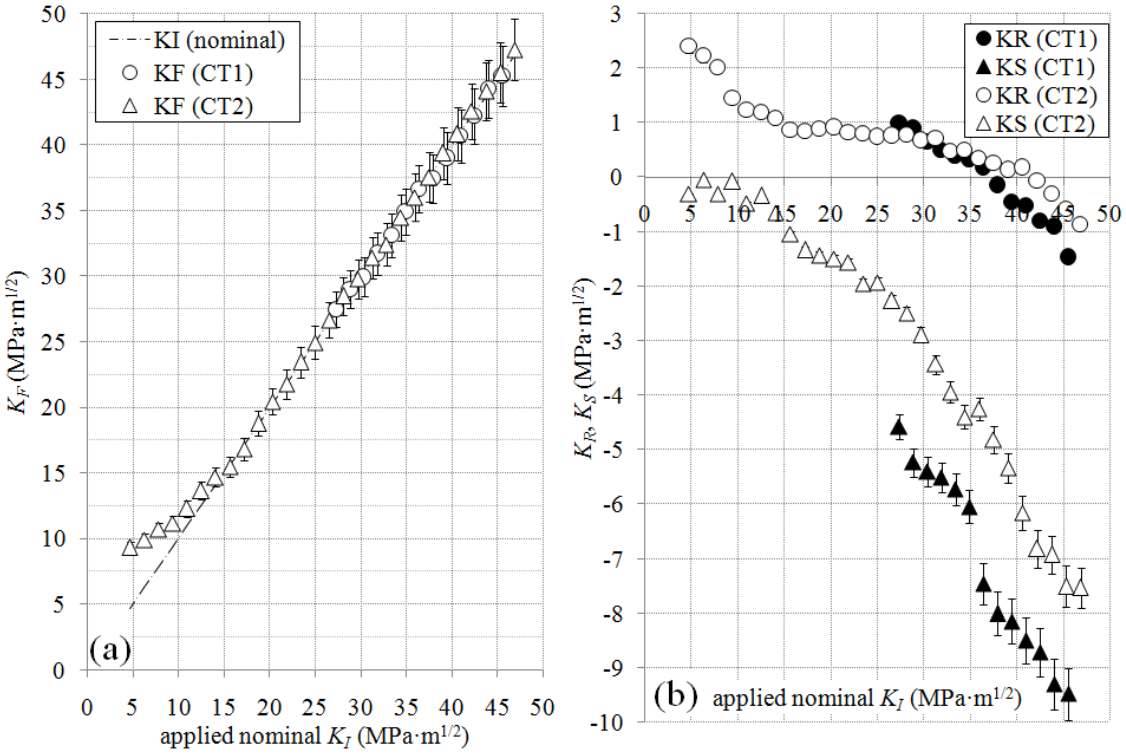

Figure 11 Values of K_F (a), K_R and K_S (b) through a loading half-cycle as a function of the applied nominal K_I for the final crack length measured in the two CT specimens (CT1R = 0.6, a = 9.20 mm and CT2 R = 0.1, a = 9.40 mm.